CORA Cork Open Research Archive
Cartlann Taighde Oscailte Chorcaí

Title	Interface roughness, carrier localization, and wave function overlap in c-Plane (In,Ga)N/GaN quantum wells: interplay of well width, alloy microstructure, structural inhomogeneities, and Coulomb effects
Authors	Tanner, Daniel S. P.;McMahon, Joshua M.;Schulz, Stefan
Publication date	2018-09-14
Original Citation	Tanner, D. S. P., McMahon, J. M. and Schulz, S. (2018) 'Interface roughness, carrier localization, and wave function overlap in c-Plane (In,Ga)N/GaN quantum wells: interplay of well width, alloy microstructure, structural inhomogeneities, and Coulomb effects', Physical Review Applied, 10(3), 034027 (19pp). doi:10.1103/PhysRevApplied.10.034027
Type of publication	Article (peer-reviewed)
Link to publisher's version	https://link.aps.org/doi/10.1103/PhysRevApplied.10.034027 - 10.1103/PhysRevApplied.10.034027
Rights	© 2018, American Physical Society. All rights reserved.
Download date	2026-11-06 06:58:57
Item downloaded from	https://hdl.handle.net/10468/7550



UCC
University College Cork, Ireland
Coláiste na hOllscoile Corcaigh

Interface Roughness, Carrier Localization, and Wave Function Overlap in *c*-Plane (In,Ga)N/GaN Quantum Wells: Interplay of Well Width, Alloy Microstructure, Structural Inhomogeneities, and Coulomb Effects

Daniel S. P. Tanner, Joshua M. McMahon, and Stefan Schulz*
Photonics Theory Group, Tyndall National Institute, University College Cork, Cork T12 R5CP, Ireland

(Received 17 April 2018; revised manuscript received 10 July 2018; published 14 September 2018)

In this work, we present a detailed analysis of the interplay of Coulomb effects and different mechanisms that can lead to carrier-localization effects in *c*-plane (In,Ga)N/GaN quantum wells. As mechanisms for carrier localization, we consider here effects introduced by random alloy fluctuations as well as structural inhomogeneities such as well-width fluctuations. Special attention is paid to the impact of the well width on the results. All calculations have been carried out in the framework of atomistic tight-binding theory. Our theoretical investigations show that independent of the well widths studied here, carrier-localization effects due to built-in fields, well-width fluctuations, and random-alloy fluctuations dominate over Coulomb effects in terms of charge-density redistributions. However, the situation is less clear cut when the well-width fluctuations are absent. For a large well width (approximately >2.5 nm), charge-density redistributions are possible, but the electronic and optical properties are basically dominated by the out-of-plane carrier separation originating from the electrostatic built-in field. The situation changes for lower well widths (<2.5 nm), where the Coulomb effect can lead to significant charge-density redistributions and, thus, might compensate for a large fraction of the spatial in-plane wave-function separation observed in a single-particle picture. Given that this in-plane separation has been regarded as one of the main drivers behind the green gap problem, our calculations indicate that radiative recombination rates might significantly benefit from a reduced quantum-well-barrier-interface roughness.

DOI: 10.1103/PhysRevApplied.10.034027

I. INTRODUCTION

Over the last several years, the theoretical and experimental analysis of carrier-localization effects in (In,Ga)N/GaN quantum wells (QWs) has been of strong interest [1–4] and has recently gathered enormous pace [5–16]. This stems from the fact that a detailed understanding of this question is important not only from a fundamental physics point of view, but also for device applications [4]. Indeed, carrier localization is widely accepted to be the reason that modern light-emitting devices based on (In,Ga)N/GaN QWs, with their high density of defects, are able to function at all [4]. Furthermore, carrier localization is essential to explain the optical properties of this material system in detail. For example, the photoluminescence (PL) spectra of these (In,Ga)N/GaN QWs exhibit large line widths [3,17], an "S-shaped" temperature dependence of the PL peak energy [1,6], a mobility edge [18], and a time-decay behavior where the explanation depends crucially on localization effects [2,9].

The cause, nature, and consequence of this localization have generated significant debate over the years. Initially, localization in (In,Ga)N was attributed to observed In-rich clusters [19], purportedly forming due to the theoretically determined immiscibility of the alloy [20]. However, careful transmission electron microscopy (TEM) [21] and detailed atomic force microscopy (AFM) measurements [22] found the observed clusters to be artifacts of the measurement technique. Additionally, when studies accounted for the strain in (In,Ga)N QWs, originating from an underlying substrate, it was demonstrated that the miscibility limit is higher than predicted from a calculation where this aspect is neglected [23]. Since these developments, carrier localization in *c*-plane (In,Ga)N QWs has been primarily attributed to random-alloy fluctuations [5,8,10–12,15], along with features introduced by the interplay of built-in field and well-width fluctuations (WWFs) [5,8,10], which have been observed in several experimental studies [3,24]. The relationship between these mechanisms of localization and the manner in which the electrons and holes are respectively localized, as well as the consequences of this localization, stand as the next challenge to the full understanding and optimization of (In,Ga)N QW-based light-emitting devices. This originates from the fact that recently two of the major roadblocks for future energy-efficient light emission from (In,Ga)N-based LEDs, namely, the

*stefan.schulz@tyndall.ie

 © 2018 American Physical Society

"green gap" and the "droop" phenomenon, have been tightly linked to carrier-localization features and interfacial roughness [7,11–13,15,25].

For instance, interfacial roughness between an (In,Ga)N QW and the GaN barrier has been considered a significant factor for increasing Auger recombination rates, as shown by Tan *et al.* [25]. Several studies have reported that Auger recombination is the main driver behind the efficiency-droop problem, which describes the reduction in the efficiency of (In,Ga)N-based LEDs with increasing current density [26–29]. In a separate theoretical study, which neglected WWFs, Jones *et al.* [12] demonstrated that, compared to virtual crystal approximation (VCA) calculations, calculations including alloy-induced carrier-localization features reveal increased Auger recombination rates in (In,Ga)N QW systems. The work of both Tan *et al.* [25] and Jones *et al.* [12] builds on the same underlying concept that *k*-selection rules are broken due to alloy/interfacial-roughness-induced localization. This highlights that understanding the effect of WWFs and alloy fluctuations on the electronic and optical properties of *c*-plane (In,Ga)N QWs in detail is not only of interest from a fundamental perspective, but also from a device-application point of view.

The understanding of these features is also relevant to the green-gap problem. This describes the drop in efficiency of (In,Ga)N/GaN emitters in the green-to-yellow spectral range when compared to blue emitters. Auf der Maur *et al.* [11] analyzed the contribution of random-alloy effects to the green-gap phenomenon. The authors [11] drew the conclusion that not only does the built-in field serve to decrease the radiative recombination rate, but so too does the in-plane separation of the carriers due to localization features induced by the random alloy. Using as a reference a calculation based on a VCA, the authors concluded that this in-plane separation contributed as much as 30% to the reduction of the radiative recombination rate in green-emitting QWs [11]. A similar conclusion was reached by Karpov using an empirical model [13].

However, it should be noted that a recent investigation by Jones *et al.* [12] contradicted this result. Using a modified continuum-based approach, accounting for random-alloy fluctuations and connected carrier-localization effects, Jones *et al.* [12] showed that random-alloy fluctuations are beneficial for the radiative recombination rate. This is based, again, on the argument that with random-alloy fluctuations, *k*-selection rules for transitions between different electron and hole states are no longer valid. Thus, even though the dipole matrix elements are reduced by carrier-localization effects and the connected spatial separation of electron and hole wave functions, a significantly increased number of transitions are allowed when compared to a VCA treatment. So, taking all this into account, the impact of carrier-localization effects on the optical properties and, in particular, on the question of the green-gap problem, which is crucial for device applications, is still surrounded by controversy, as is the underlying physics of these systems in general.

In addition to their disagreement on the impact of alloy fluctuations on the radiative recombination in (In,Ga)N devices, these previous theoretical studies have also neglected two important aspects of typical (In,Ga)N/GaN QWs. First, above discussed studies do not account for structural inhomogeneities such as WWFs. These structural features, in tandem with the strong built-in fields in *c*-plane (In,Ga)N QWs, have been found to localize electron wave functions [8,30] and can therefore strongly contribute to the in-plane carrier separation. If the in-plane carrier-localization features are central to the green-gap problem, then WWFs, by inducing further in-plane separation, should worsen the reduction in efficiency. Therefore, a detailed understanding of the impact of the interface roughness is required for the optimization of devices to ameliorate the green-gap problem.

Second, an additional component of the study of the importance of in-plane carrier localization for optical properties is Coulomb effects. These effects have been widely neglected in the theoretical studies that account for carrier-localization features in (In,Ga)N/GaN QWs. This leads to the question of whether or not Coulomb effects can reduce the in-plane carrier separation. Given that the electrostatic built-in field strongly spatially separates electron and hole wave functions along the growth direction, the importance of Coulomb effects should increase with decreasing well width. In this respect, the question remains if carrier localization due to the combination of WWFs, built-in field, and random-alloy fluctuations dominates over the attractive Coulomb interaction between electron and hole. Most of the theoretical studies discussed here have been based on either single-particle results [5,10–12,14], in the absence of WWFs, or for a fixed well width [11,12,14]. In studies including Coulomb effects and carrier localization, systems with a fixed well width and a high In content of 25% have been investigated so far [8].

Finally, if Coulomb effects do indeed gain significance when structural well parameters change, the recombination dynamics of the system could change drastically, which again could be of benefit for (In,Ga)N-based devices via improved radiative recombination rates. An important early connection between carrier-localization mechanisms and the distinct optical properties of (In,Ga)N/GaN QWs was demonstrated by Morel *et al.* [2]. Here, Morel and coworkers [2] applied a model of independently localized electrons and holes (a pseudo-two-dimensional donor-acceptor pair system) to describe the *nonexponential* decay curves in time-resolved PL measurements of *c*-plane (In,Ga)N/GaN QW systems. In contrast, other studies on *c*-plane (In,Ga)N/GaN QWs reported time-resolved PL measurements in which the PL decay curves exhibit a *single-exponential* behavior [31]. Such behavior can

be attributed to exciton localization effects, where, for instance, the hole is strongly localized and the electron localizes about the hole [9]. Therefore, as already indicated above, the recombination dynamics (nonexponential vs single exponential) can be affected and ideally may be tuned by a variety of different factors such as well width [31]; In content [32,33]; or, as we will show, the interface roughness. Taking all of the above into consideration, understanding the interplay of Coulomb effects, interfacial roughness, and carrier-localization mechanisms is obviously interesting from a fundamental physics viewpoint but is also key for device design.

In this work, we undertake the analysis of the interplay of carrier-localization mechanisms, introduced by (random) alloy fluctuations, WWFs, and Coulomb effects and we comment here on the connected impact on the optical (radiative) properties of (In,Ga)N/GaN QWs. Special attention is paid to the influence of the well width on the results. The calculations have been carried out in an atomistic tight-binding (TB) framework, allowing us to gain insight into these questions on a microscopic level.

Here, we have studied *c*-plane (In,Ga)N/GaN QWs with a well width varying between 1.6 and 3.43 nm. For this analysis, we have used an "intermediate" In content of 15%. By studying identical QWs with and without WWFs, we demonstrate the significant impact that WWFs have on the localization of electron states, even for a smaller well width (1.6 nm). Independent of well width, this picture is mainly unchanged when Coulomb effects are included and carrier-localization features remain dominated by WWFs (electron) and random-alloy fluctuations (hole). For higher In contents, usually realized for emitters operating in the green spectral range, this effect will be even more pronounced [10].

The situation in the absence of WWFs is less clear cut. Here, the single-particle electron wave function exhibits a more delocalized nature with perturbations introduced by the local alloy structure. When including Coulomb effects, even for the larger well width, our calculations reveal a redistribution of the electron charge density. When turning to systems with a lower well width, Coulomb effects can significantly affect the in-plane carrier separation. Here, we observe that, in the absence of the WWFs, the electron wave function is much more likely to localize about the hole, thus resulting in exciton-localization-like features. Overall, when looking at optical spectra, the benefits of this charge-density redistribution are found to increase with decreasing width. This indicates that the out-of-plane separation of the carriers dominates the wave function overlap at larger widths.

In general, our results show that reducing the interface roughness between GaN and (In,Ga)N in (In,Ga)N/GaN QWs, and thus ideally circumventing WWFs, should, due to Coulomb effects, reduce the in-plane spatial separation of electron and hole wave functions. Following the results of Auf der Maur *et al.* [11], the radiative recombination rate should benefit from this. Additionally, in the light of the arguments given by Jones *et al.* [12], an increased wave function overlap along with the absence of *k*-selection rules should give a further improvement of the radiative recombination rate. Thus reducing the (In,Ga)N/GaN interface roughness could be a promising way forward to improve the radiative device characteristics of (In,Ga)N/GaN based light emitters across a wide range of emission wavelength.

The manuscript is organized as follows. In the following section, we briefly review the theoretical framework used in our studies. Here, the QW system and how WWFs and alloy microstructure are treated is also discussed. Section III presents the results of our theoretical study. In a first step, Sec. III A, the impact of random-alloy fluctuations and WWFs on the built-in potential are discussed. This is followed by the analysis of single-particle results in Sec. III B. The impact of Coulomb effects on optical properties is discussed in Sec. III C. In Sec. III D, we compare and relate our theoretical findings to experimental data, radiative recombination dynamics, and the connected importance for nitride-based optoelectronic devices. Finally, in Sec. IV, a summary and conclusions of our investigations are presented.

II. THEORY AND QUANTUM WELL SYSTEM

In this section we briefly review the theoretical framework and the QW model system applied in this work. We start in Sec. II A with the theoretical framework. In Sec. II B, the supercell used in our calculations is introduced. Here, we discuss also aspects such as In-atom distribution as well as structural inhomogeneities (well-width fluctuations).

A. Theoretical framework

The full description of each of the ingredients of our theoretical framework has been presented in detail in our previous work [8]. Here, we summarize only the main points. The central component underlying our study of the electronic and optical properties of (In,Ga)N/GaN QWs on an atomistic level is a nearest-neighbor sp^3 tight-binding (TB) model. This model takes input from a valence force field (VFF) model, implemented in LAMMPS [34]. The applied VFF approach is based on Martin's model, introduced in Ref. [35], including therefore electrostatic effects. This model accurately captures deviations from the ideal wurtzite structure, such as the lattice constant c/a ratio. Given the atomistic nature of our VFF approach, the model takes into account that the number of In and Ga atoms in the nearest-neighbor environment of a N atom varies. Using the VFF, the relaxed atomic positions in the alloyed and strained supercell can be determined, including therefore also alloy induced local variations in

the bond length and corresponding strain fields. These relaxed atomic positions provide input for the strain corrections of the TB matrix elements [36]. Additionally, the relaxed atomic positions provide input for our recently developed local polarization theory [36]. In this approach, the total polarization vector field is divided into a macroscopic and local polarization contribution. The macroscopic part is related to clamped-ion contributions (no relaxation of the internal degrees of freedom of the atoms), while the local part is evaluated per local tetrahedron, accounting therefore for internal strain effects. Starting from the local polarization at the different lattice sites, the resulting built-in potential is calculated from a point dipole model. This method circumvents the problem of solving Poisson's equation on a (nonuniform) wurtzite lattice, keeping in mind the relaxed atomic positions of the (In,Ga)N QW. The calculated built-in potential is included in the TB model as a site-diagonal correction, which is a widely used approximation [37–39]. It should be noted that, here, we are interested in the low-carrier-density regime (see below). Focusing on this regime helps to disentangle carrier-localization effects arising from WWFs, alloy microstructure, and Coulomb effects, thus throwing light on the interplay of these different aspects. Therefore, a non-self-consistent TB calculation is sufficient for our purposes here. However, to account for potential charge-carrier-density redistributions, which could be important, for instance, for the green-gap problem, as highlighted above in more detail, we include Coulomb effects in our calculations.

To include Coulomb effects, the TB single-particle states serve as input for configuration interaction calculations [40]. The calculations are restricted to excitonic effects, meaning that only one electron-hole pair is considered. We account here for the direct electron-hole interaction; exchange terms are neglected since the connected matrix elements are small compared to the direct part. To account for screening effects in the Coulomb interaction, which is intrinsically a complex problem [41,42], we use here a simplified approach and assume an isotropic and material-independent (static low-frequency) dielectric constant. For GaN, we employ the values from Nakamura and Chichibu ($\epsilon^r_{\perp,0} = 7.87$, $\epsilon^r_{\parallel,0} = 8.57$), resulting in a very good agreement between theory and experiment in terms of GaN exciton-binding energies [43]. For InN, we use the values from Ref. [44] ($\epsilon^r_{\perp,0} = 13.1$, $\epsilon^r_{\parallel,0} = 14.4$). Given that both for InN and GaN the vales of the ordinary ($\epsilon^r_{\perp,0}$) and extraordinary ($\epsilon^r_{\parallel,0}$) component are very similar in magnitude, the isotropic approximation is reasonable. To obtain the (In,Ga)N dielectric constant, a linear interpolation between the InN and GaN values is applied. For the Coulomb calculations, this averaged dielectric constant is used for the entire supercell, justified by the observation that electron and hole wave functions are mainly localized inside the QW region (see below). Furthermore, as we will discuss below, we will study here only moderate In contents so that the dielectric constant contrast between well and barrier is small. Thus, the assumption of a position-independent dielectric constant is a reasonable first approximation. Given that the screening of the Coulomb interaction should be distance dependent, our Coulomb matrix elements are split into a short-range and long-range part [45]. The short-range, on-site part is unscreened, while for the long-range part, the above approximation for the screening has been used. Similar approaches and approximations have been made in other systems [45–47]. In addition to Coulomb matrix elements, the TB wave functions have also been used to calculate dipole matrix elements [8,48]. In connection with many-body wave functions and via Fermi's golden rule, the dipole matrix elements are used to calculate optical spectra. More details are given in Refs. [8,48].

B. Quantum well structure and simulation supercell

The TB calculations have been performed on wurtzite supercells with approximately 82 000 atoms. This corresponds to an overall system size of $10 \times 9 \times 10$ nm^3 with periodic boundary conditions. The QW width inside the supercell has been varied to investigate the impact of this quantity on the electronic and optical properties of the system. The well width, L_w, is set to $L_w = 1.6$ nm, $L_w = 2.11$ nm, $L_w = 2.65$ nm, and $L_w = 3.43$ nm. As mentioned above, we are interested in investigating the influence of the well width on the electronic and optical properties of (In,Ga)N/GaN QWs; to do so, we keep the In content in the QW region fixed at 15%. Based on experimental studies [21,49], we distribute In atoms randomly in the active region of the QW. It is important to note that, in our atomistic framework, the In content at the QW-barrier interface will locally vary. But, we do not account here for penetration of In atoms into the barrier. In the literature, different In-atom-distribution profiles have been considered. Yang *et al.* [7] and McBride *et al.* [50] considered a Gaussian alloy distribution along the growth direction of *c*-plane (In,Ga)N QWs. However, several experimental studies have reported a sharp lower QW barrier interface [growth of (In,Ga)N on GaN], while the upper interface [GaN on (In,Ga)N] exhibited WWFs and some penetration of In into the barrier [49,51–55]. Watson-Parris [30] considered the effect of In incorporation in the barrier at the upper interface for a fixed well width (2.85 nm) and In content (25%) on the basis of a modified continuum-based model, concluding that the inclusion of a diffuse upper interface has no noticeable effect on the results in terms of carrier localization. This indicates that, for our present study, the penetration of In atoms into the barrier is of secondary importance. This is further supported by the fact that the diffuseness of the In atoms in the QW plane is homogeneous [5]. Thus, one could expect that the experimentally

observed WWFs have a more significant impact on carrier-localization effects when compared to the penetration of In atoms into the barrier. Finally, it should be noted that recent experimental studies have shown that by a careful choice of the growth procedure, the In incorporation in the barrier can significantly be reduced [55]. Therefore, the assumptions made here about the In distribution in the well and at the QW barrier interface should provide a good description of the experimentally observed systems.

In order to analyze the impact of the alloy microstructure on the results, the calculations have been repeated 20 times for each L_w value. To closely compare the results from the same configuration for different QW widths L_w, we proceed in the following way. We start with the lowest L_w values and generate the 20 different microscopic configurations. When studying the next largest system, for each configuration, we keep the random In atom configuration and just add new layers to the existing QW structure. For instance, for configuration (Config.) 1 of a QW of width $L_w = 2.11$ nm, the placement of In atoms in the first 12 atomic layers is identical to the placement of In atoms in the first 12 layers of the $L_w = 1.6$ nm system for the same configuration. Likewise, the first 20 atomic layers of Config. i of the $L_w = 2.85$ QW have identical In-atom distributions to the 20 atomic layers in Config. i, forming the well with $L_w = 2.11$ nm. Thus, in terms of the In-atom distribution, the lower QW-barrier interface is always the same for a given microscopic configuration, independent of the QW well width. In this way, we are able to partially isolate the effects of well width and WWFs on the electronic and optical properties of the here considered $In_{0.15}Ga_{0.75}N/GaN$ QWs from random-alloy effects. Finally, all calculations have been performed in the presence and absence of WWFs. For the WWFs, following previous work [5,8,10,30], we assume disklike WWFs. The diameter of these fluctuations is assumed to be 5 nm, with a height of two monolayers, which is consistent with experimental observations [3,24]. In total, 320 atomistic calculations are performed to study the interplay of Coulomb effects, well width, and carrier localization due to WWFs and random-alloy fluctuations on the electronic and optical properties of $In_{0.15}Ga_{0.85}N/GaN$ QWs.

III. RESULTS

In this section, we present the results of our atomistic analysis of the impact of well width and WWFs on the electronic and optical properties of c-plane (In,Ga)N/GaN QWs. Before turning to the electronic and optical properties, we start our discussion with a study of the electrostatic built-in potential and how alloy and WWFs affect this quantity. This investigation is presented in Sec. III A. Having discussed the built-in potential, we turn and present in Sec. III B the results of our TB analysis in the absence of Coulomb effects (single-particle data). In Sec. III C, we discuss the impact of Coulomb (excitonic) effects on the results. Finally, we relate the theoretical results obtained here to experimental observations (Sec. III D).

A. Impact of random-alloy and well-width fluctuations on the built-in potential

To establish the impact of alloy and WWFs on the electrostatic built-in potential, V_p, Fig. 1 displays contour plots of V_p for different slices through the supercell of the same arbitrarily chosen microscopic configuration. The potential displayed is that of a QW of width $L_w = 2.65$ nm. The contour plots are shown in the x-z plane, where z is parallel to the wurtzite c-axis. The y-coordinate is varied, with increasing magnitude from left to right, resulting then in the different slices depicted in subsequent columns of Fig. 1. As a guide to the eye, the (white) dashed lines indicate the QW interfaces. To ascertain the impact of interface roughness on the built-in potential, the upper row displays the result for a QW with a WWF (V_p^{WWF}); the middle row gives the same QW configuration without a WWF ($V_p^{\mathrm{No\ WWF}}$); and the last row shows the difference in the potential between a QW with and without a WWF, $\Delta V_p = V_p^{\mathrm{WWF}} - V_p^{\mathrm{No\ WWF}}$. Several features of the built-in potential are now of interest for our analysis.

First, in contrast to standard 1-D continuum-based approximations, which treat (In,Ga)N/GaN QW systems as an ideal system that can be described by average parameters, the built-in potential is strongly position dependent. This position dependence is manifested in Fig. 1 as isolines which are nonparallel. This is in contrast to the parallel isolines expected from a 1-D continuum-based, capacitorlike picture, where the potential is constant outside the well and has a well-defined slope inside. Thus, the corresponding field is zero in the barrier and constant inside the QW. Second, the alloy fluctuations lead also to "pockets" in which the built-in potential significantly varies with respect to its environment. From this, we infer already that random-alloy fluctuations lead to significant changes in the built-in potential, both on a macroscopic and on a local, microscopic level. Third, turning now to the impact of the WWF: As expected, in the region of the WWF, the built-in potential changes compared to the situation without the WWF. However, when looking at the last row of Fig. 1, we find also that the built-in potential underneath the WWF changes significantly compared to the situation in which no WWF has been considered. This originates from the fact that the disklike WWF is a three-dimensional object and that the strain field around this "QD-like" structure is changed. This has several consequences. Given that electron wave functions are localized at the upper interface of the QW and that the (alloy) microstructure of the upper layer with the inclusion or exclusion of a WWF changes, carrier-localization features of these states are expected to be strongly affected. What

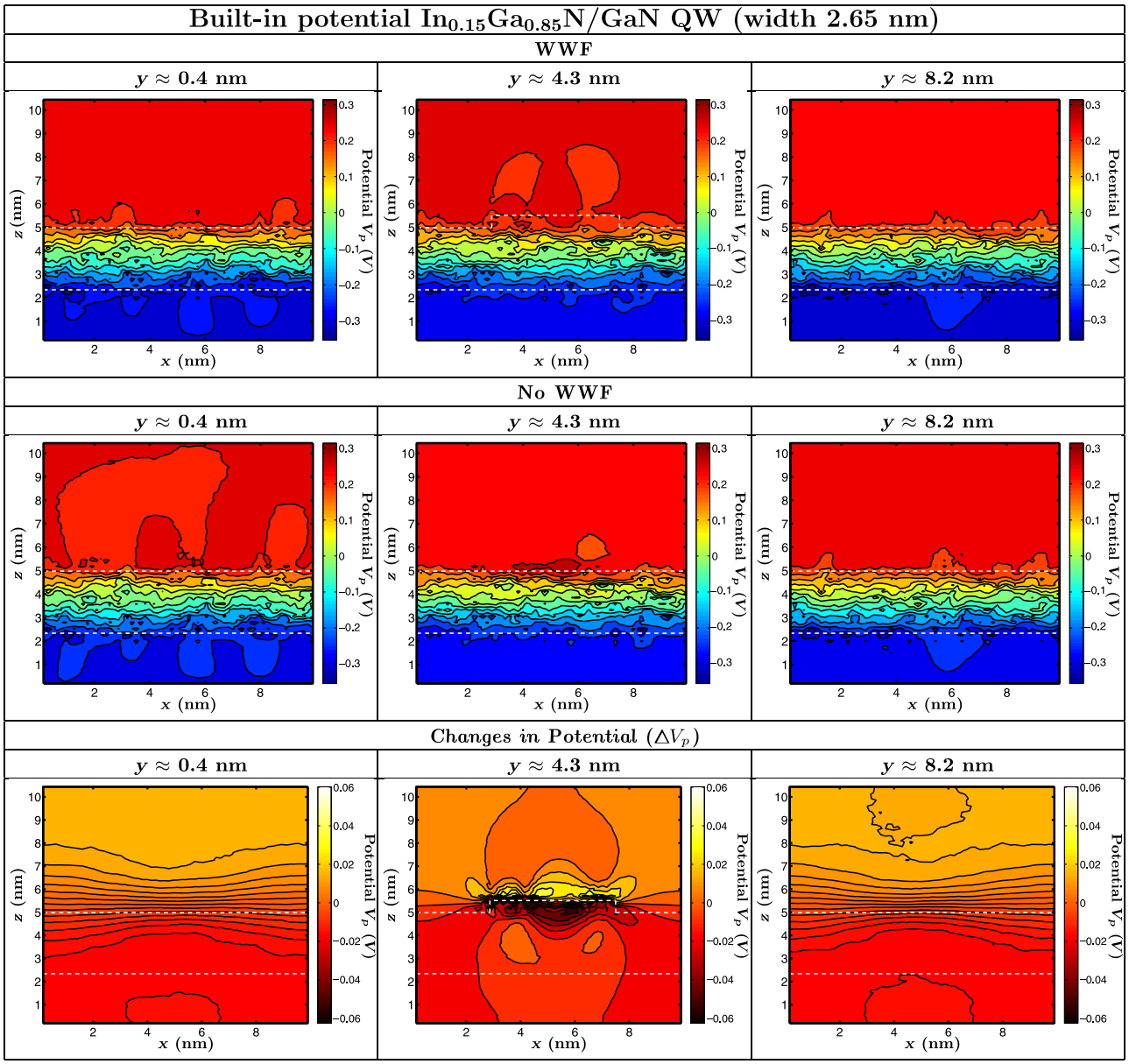


FIG. 1. Contour plots of the electrostatic built-in potential V_p in the x-z plane of an $In_{0.15}Ga_{0.85}N/GaN$ quantum well with well width $L_w = 2.65$ nm. The z-axis is parallel to the wurtzite c-axis. The results are shown for different slices ($y = 0.4$ nm, $y = 4.3$ nm, $y = 8.3$ nm) through the supercell of the same arbitrary microscopic configuration. The first row depicts the data for the quantum well where a disklike well width fluctuation is taken into account (WWF). The middle row displays the results for the same configuration and slices through the same planes as in the first row, however, this time, in the absence of the well-width fluctuation (No WWF). The last row depicts the difference in the potential $\Delta V_p = V_p^{\mathrm{WWF}} - V_p^{\mathrm{No\ WWF}}$ between the situation with (V_p^{WWF}) and without ($V_p^{\mathrm{No\ WWF}}$) the well-width fluctuation calculated at the different y-coordinates.

might be less straightforward to predict *a priori* is that, even though the alloy microstructure at the lower interface is not changed in our approach here (cf. Sec. II B), the hole states, which are localized at this interface, can be affected by the three-dimensional built-in potential effects discussed above. This aspect will be more pronounced in narrower wells. Therefore, introducing WWFs affects not only the effective volume of the QW, but also produces built-in potential modifications originating from the altered microscopic alloy configuration and strain relaxation of the system. Overall, the inclusion of the WWF also leads to a slight increase in the macroscopic built-in field compared to the system without WWFs. This is based on the observation that ΔV_p is slightly negative (positive) below (above) the well (cf. the last row of Fig. 1). Equipped with this knowledge, we turn now to analyze the electronic structure

of (In,Ga)N/GaN QWs in the presence and absence of WWFs. Special attention is paid to the impact of the well width L_w on the results. This will be the topic of the next two sections. We begin our analysis in the next section with an examination of single-particle results.

B. Impact of well width, random alloy and well-width fluctuations on the electronic structure: Single-particle results

Figure 2 shows the single-particle (a) electron and (b) hole ground state (GS) energy as a function of the microscopic configuration number (Config. No.). The zero of energy for all these calculations is the unstrained GaN valence band edge. The data are shown for the different well-width values ranging from $L_w = 1.6$ nm to $L_w = 3.43$ nm. The results where WWFs have been considered in the calculations are given by the filled symbols, while the open symbols display the data in the absence of WWFs (No WWF). Overall, two important features should be taken into account before starting the detailed analysis of Fig. 2. First, because of the presence of the electrostatic built-in field along the growth direction (cf. Fig. 1), electron and hole wave functions are localized at opposite interfaces of the QW: electrons at the upper interface and holes at the lower interface [5]. Second, it is important to remember that WWFs are introduced at the upper QW interface. Thus, from a structural point of view, the lower interface for a given microscopic configuration is unchanged when introducing the WWF. From this perspective, mainly electron GS energies should be affected by WWFs. Equipped with this information, several general features can be deduced from Fig. 2.

For both electrons and holes, the GS energies vary significantly with configuration number, though the holes show a much greater variance. This indicates that the alloy microstructure of the systems plays an important role. Additionally, for all widths L_w, the inclusion of the WWF shifts the electron GS energies to lower energies [cf. Fig. 2(a)]. Similarly for the hole GS energies [cf. Fig. 2(b)], for all configurations but one (Config. 18), the inclusion of the WWF leads to a shift to higher energies. We will come back to the particularities of Config. 18 further below.

For the electrons [Fig. 2(a)], we attribute the decrease in the GS energies to the slight increase in QW volume due to the WWFs and the overall slightly stronger built-in field in the system with WWFs when compared to structures without a WWF (cf. Sec. III A). Turning to the hole GS energy, even though the alloy microstructure at the lower interface is not changed here by the addition of a WWF, the changes in the QW volume and the connected changes in built-in field due to the presence of the WWF (cf. Sec. III A) also affect the hole GS energy. However, when considering a given configuration, the changes in the hole GS energies

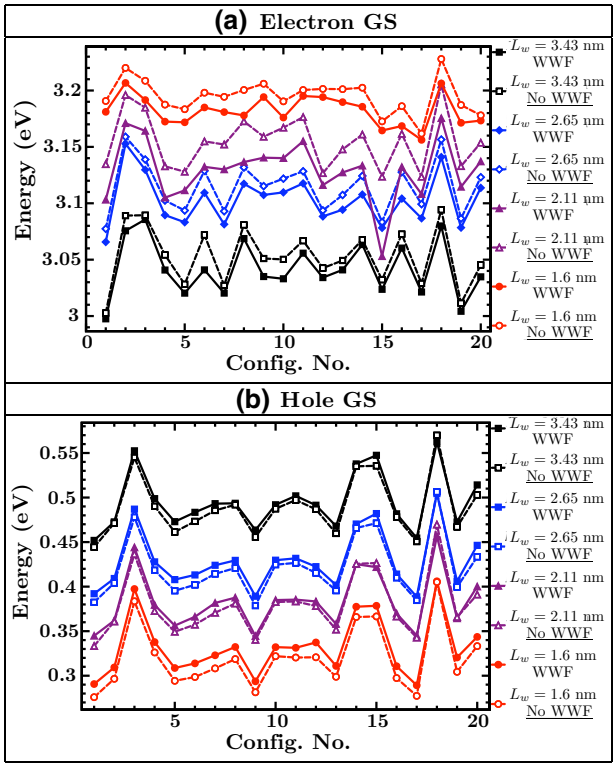


FIG. 2. Single-particle (a) electron and (b) hole ground-state (GS) energy as a function of the microscopic configuration number (Config. No.). The data from calculations including well-width fluctuations (WWF) are given by the filled symbols; the results when the well-width fluctuation is absent are denoted by the open symbols (No WWF). The data are displayed for the different well widths L_w.

due to the presence of a WWF are in general smaller when compared to the changes in the electron GS energies.

The resulting changes in the electron and hole GS energies due to the presence of WWFs are summarized in Fig. 3. Here, the GS *transition energy* for the different well widths is displayed as a function of the microscopic configuration number (Config. No.). For all well widths L_w, we observe a redshift in the transition energy due to the presence of WWFs. This behavior reflects the trends in the electron and hole GS energies. This finding is also consistent with the simple picture that, by including the WWF, the well becomes effectively wider and that the built-in field slightly increases when compared to the QW without a WWF. Additionally, as expected from our analysis above, the GS transition energy varies significantly as a function of the configuration number. This behavior is consistent with the experimentally observed broad PL spectra in (In,Ga)N/GaN QWs [3,56,57].

Having established general features of how alloy fluctuations and WWFs affect both electron and hole GS energies in a single-particle picture, we turn now and look at excitonic effects. Initially, we present an analysis of the

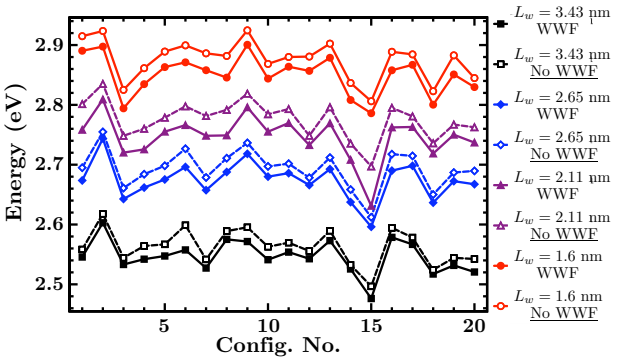


FIG. 3. Single-particle ground-state transition energies as a function of the microscopic configuration number (Config. No.). The results are given for the different well widths L_w. Data in the absence of the well-width fluctuation (No WWF) are denoted by the open symbols, while data in the presence of the well-width fluctuation (WWF) are given by the filled symbols.

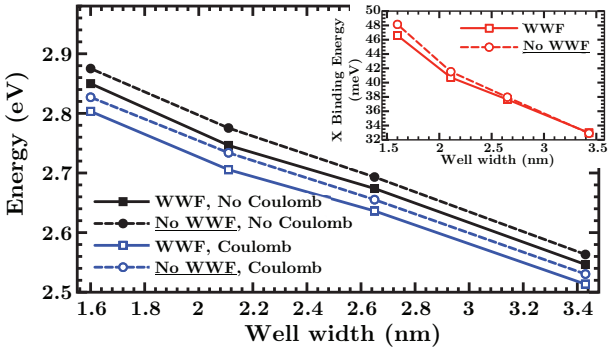


FIG. 4. Average ground-state transition energies with (WWF, squares) and without (No WWFs, circles) well-width fluctuations as a function of the well width L_w. The data in the absence of Coulomb effects are given by the respective filled symbols, while the open symbols denote the results when excitonic effects are taken into account. Inset: Exciton (X) binding energies in the presence (WWF, open squares) and absence (No WWF, open circles) of well-width fluctuations as a function of the well width L_w.

(average) transition energy and also the exciton binding energy. In a second step, we discuss how the Coulomb effect impacts carrier-localization features.

C. Impact of well width, random alloy and well-width fluctuations on the electronic and optical properties: Excitonic effects

Figure 4 displays the *average* GS transition energies in the presence and absence of WWFs as a function of the well width L_w. Additionally, results with and without the inclusion of Coulomb effects in the calculations are given. The open (filled) symbols denote the results in the presence (absence) of excitonic effects. The squares (circles) show the data when WWFs are included in (excluded from) the calculations. Thus, the filled symbols in Fig. 4 are obtained from averaging over the 20 different microscopic configurations presented in Fig. 3. The filled symbols in Fig. 4 confirm in a simple manner the aforementioned conclusion that the inclusion of WWFs result in a redshift of the transition energies. Figure 4 also illustrates clearly the increase in transition energy with decreasing L_w. Such a behavior is expected from a simple particle-in-box-like picture. Looking at the open symbols, we see that these expected trends also hold in the case where Coulomb effects are included.

Additionally, a comparison of the average transition energy with and without Coulomb effects allows for a first insight into the question of how the Coulomb interaction affects the optical properties of QWs with different structural parameters. To facilitate this investigation, the inset in Fig. 4 depicts the exciton (X) binding energy in the presence (square) and abesence (circle) of WWFs, as a function of L_w. Here, the exciton binding energy is defined as the difference in the average single-particle GS transition energy and the calculated average excitonic transition energy. Three important features can be extracted from this inset: (i) the exciton binding energy increases with decreasing L_w; (ii) in general, the exciton binding energy decreases with the inclusion of WWFs; and (iii) the impact of the WWF on the exciton binding energy decreases with increasing L_w and turns out to be of secondary importance for large L_w. These results can be explained in terms of wave-function overlaps: In a simplified picture, one expects that the lower the spatial wave function overlap, the lower the exciton binding energy. Thus, the decreasing vertical spatial separation of electron and hole wave functions with decreasing L_w accounts for the increase in the exciton binding. Secondly, if the electron wave functions are localized independently of L_w by the WWFs, then a further in-plane spatial separation, in addition to the out-of-plane separation by the electrostatic built-in field, is expected. This in-plane separation can then lead to a further decrease in the exciton binding energy when comparing the system with and without WWFs. Finally, the finding that removing the WWF has a reduced effect on the binding energies in wider than in narrower wells is due to the fact that the strength of the Coulomb interaction is determined primarily by the vertical separation between the carriers. The fact that, for larger values of L_w ($L_w > 2.5$ nm), the average exciton binding energy is almost unaffected by the WWF leads to the following interesting conclusion. Assuming that WWFs lead to an additional in-plane spatial separation between the carriers compared to a system without WWFs, the results of Fig. 4 indicate that the in-plane separation between the carriers is of secondary importance, at least in terms of the exciton binding energy. We will come back to this point in Sec. III D, when we compare our theoretical data with experimental results and

connect our theoretical findings also to radiative recombination characteristics. It should be noted that additional factors, such as the density and the statistical variations in size and shape of WWFs, could affect this result. These factors could further increase the in-plane spatial-separation contribution.

So far, we have only discussed *averaged* results and made assumptions about the nature of the carrier-localization features. To corroborate these explanations of observed trends in the averaged properties and to investigate the interplay among well width, alloy microstructure, structural inhomogeneities, and Coulomb effects, we present next an analysis of the electronic structure of the different QWs for different microscopic configurations. Figure 5 displays the exciton binding energies as a function of the configuration number (Config. No.). Here, we have focused our attention on the extreme well-width cases, thus, $L_w = 1.6$ nm (red circles) and $L_w = 3.43$ nm (black squares). The other well-width systems considered here then reflect an intermediate situation. The results in the absence of WWFs (No WWFs) are always indicated by open symbols (squares or circles), while the results where WWFs are taken into account are denoted by the filled symbols. We start our analysis here by looking at the QW system with $L_w = 3.43$ nm (black squares). When comparing the exciton-binding energies obtained in the presence and absence of WWFs, we find that the WWF is of secondary importance for this quantity. This finding is consistent with the results of the average exciton binding energy depicted in the inset of Fig. 4. This indicates already that, for wider QWs, the wave-function overlap is not significantly affected by the presence of WWFs. Again, we will come back to this question below when we discuss the interplay of WWFs and Coulomb effects on the wave functions/charge densities. For the system with $L_w = 1.6$ nm, the results are given by the (red) circles in Fig. 5. In contrast to the system with $L_w = 3.43$ nm, we observe that the presence of WWFs can make a noticeable difference to the exciton binding energy in the different configurations. However, there is not a universal trend in the sense that WWFs always lead to a decrease in the exciton binding energy. We also have situations where the WWF leads to an increase in the exciton binding energy (e.g., Configs. 18 and 19). Overall, this reveals that for smaller L_w values, the presence or absence of WWFs in combination with Coulomb effects significantly affects the electron-hole overlap. For larger well widths, this seems not to be the case, since the exciton-binding energies are almost unaffected by the presence of WWFs compared to the situation where WWFs are absent (cf. Fig. 5).

To shed more light on wave-function localization features and to support explanations given earlier in terms of wave-function overlaps, we now turn to examine the single-particle and many-body (excitonic) charge densities of the considered QWs. Figures 6 and 9 display

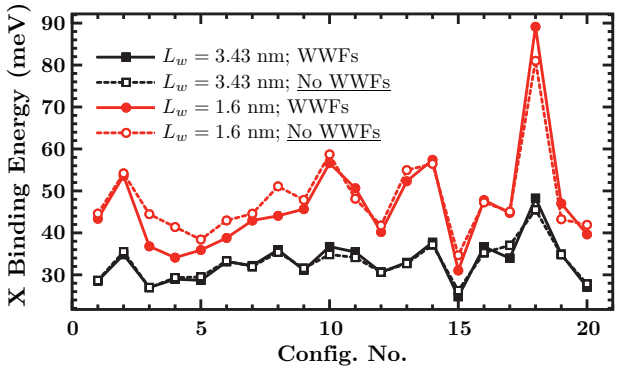


FIG. 5. Exciton (X) binding energy as a function of the microscopic configuration number (Config. No.). The results are shown for a well width of $L_w = 1.6$ nm (red circles) and $L_w = 3.43$ nm (black squares), respectively. The open symbols denote the results in the absence of well-width fluctuations (No WWFs), while the filled symbols denote the data when well-width fluctuations (WWFs) are taken into account.

isosurface plots of the electron and hole GS charge densities in the presence and absence of WWFs for the QWs with $L_w = 3.43$ nm and $L_w = 1.6$ nm, respectively. Here, the results are displayed both for the single-particle states (Single-Particle) and when Coulomb interaction effects (Many-Body) are taken into account. The excitonic charge densities have been constructed from reduced density matrices [8,58]. For both systems, the results are shown for a side view (perpendicular to the c-axis) and for a top view (parallel to the c-axis). The isosurfaces of the charge densities are displayed at 10% (light surface) and 50% (dark surface) of the respective maximum probability densities. Electron charge densities are given in red, hole charge densities in blue. To understand general features, we have selected configurations 4, 11, and 18. These configurations have been selected on the basis of the system with $L_w = 1.6$ nm, since they reflect situations where the WWF leads to a reduction (Config. 4) and an increase (Config. 18) of the exciton binding energy (cf. Fig. 5). The last configuration, Config. 11, represents the situation where the exciton binding is almost unaffected by the presence of WWFs (cf. Fig. 5).

We start our analysis with the QW system of width $L_w = 3.43$ nm. The charge densities of the above discussed configurations are displayed in Fig. 6. In a first step, we look at the single-particle results with and without WWFs (the two left columns in Fig. 6). Firstly, because of the presence of the electrostatic built-in field, electron and hole wave functions are separated to opposite interfaces of the QW. Consistent with previous calculations [5,8,11,12], we find here very strong hole localization effects due to random-alloy fluctuations. Keeping in mind that for a given microstructure (configuration), the local alloy arrangement at the lower interface is not changed

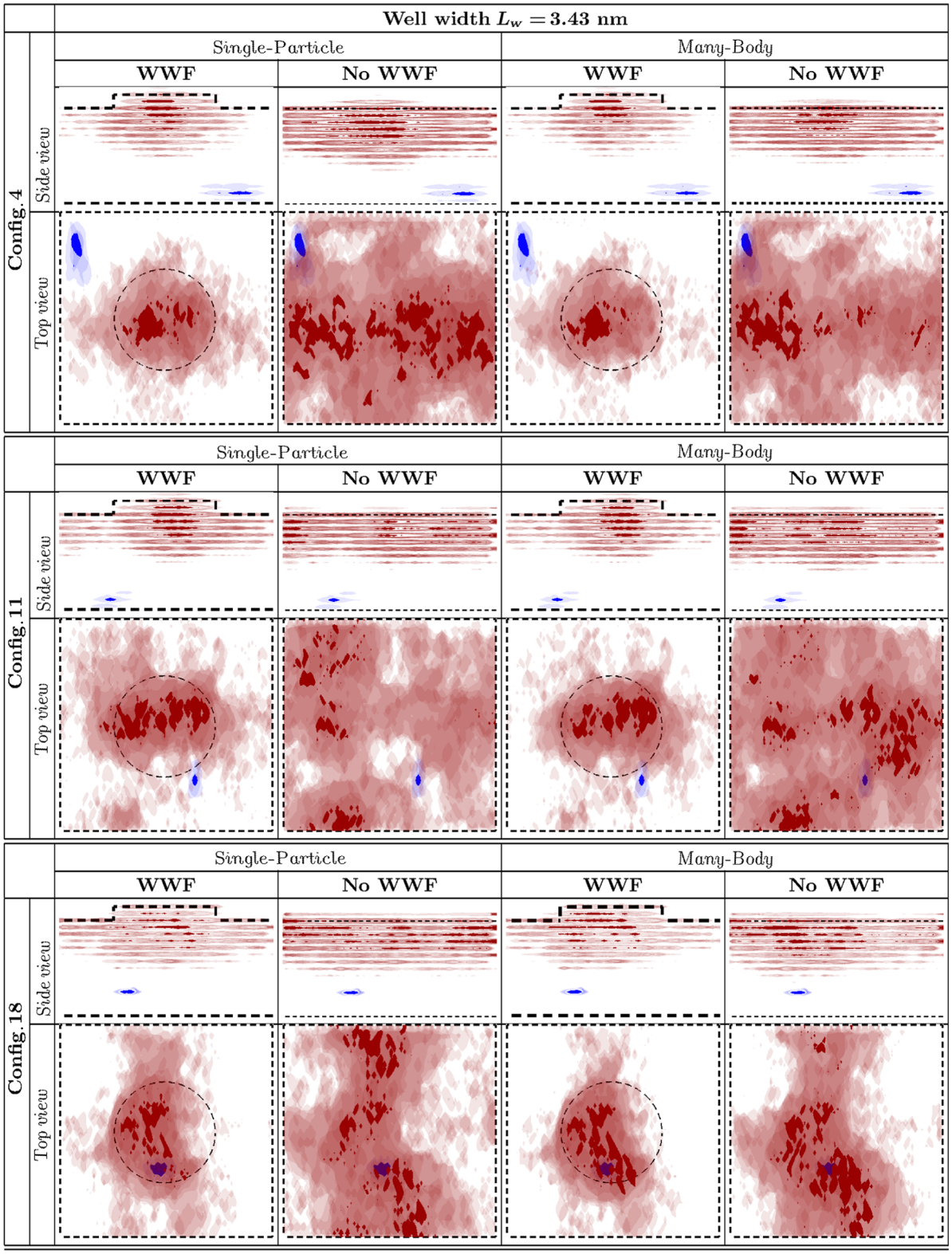


FIG. 6. Isosurface plots of electron (red) and hole (blue) ground-state charge densities in the absence (Single-Particle, left) and presence (Many-Body, right) of Coulomb (excitonic) effects for different microscopic configurations and different viewpoints. The side view is perpendicular to the c-axis, and the top view is parallel to the c-axis. The light (dark) isosurfaces correspond to 10% (50%) of the maximum charge density. Results are shown with (WWF) and without (No WWF) well-width fluctuations. The well width L_w here is $L_w = 3.43$ nm.

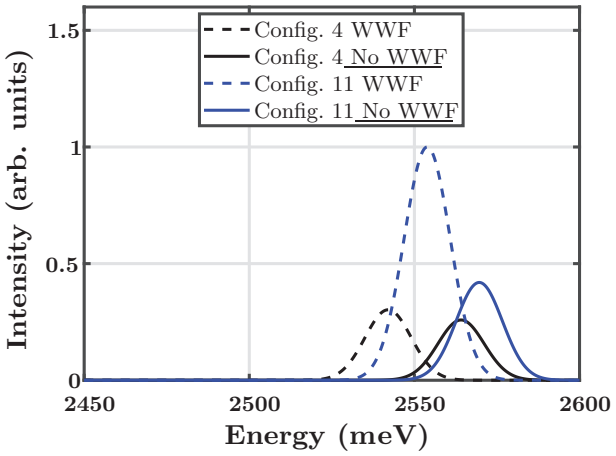


FIG. 7. Emission spectrum, neglecting Coulomb effects (single-particle), for Configs. 4 (black) and 11 (blue) in the presence (dashed lines) and absence (solid lines) of well-width fluctuations. The well width of the system is $L_w = 3.43$ nm. The data are normalized to Config. 11 in the presence of well-width fluctuations (WWF).

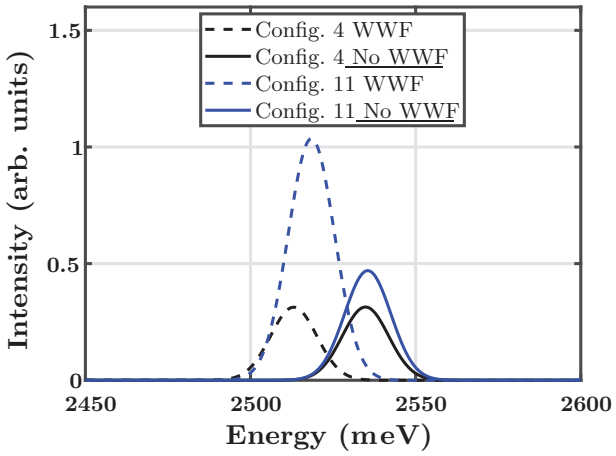


FIG. 8. Excitonic emission spectrum for Configs. 4 (black) and 11 (blue) in the presence (dashed lines) and absence (solid lines) of well-width fluctuations. The well width of the system is $L_w = 3.43$ nm. The data are normalized to the spectrum of Config. 11 in the absence of Coulomb effects but in the presence of the well-width fluctuation (WWF).

when including the WWF, the hole wave function remains localized in the same spatial position when comparing the results in the presence and absence of the WWF for the same configuration. However, we observe that the localization features of the electron wave functions, for all configurations, are changed due to the presence of the WWF. We find that the electron wave function is always localized at the upper interface by the WWF. This is consistent with previous theoretical studies [5,8,30]. In the absence of the WWF, the electron wave function is more delocalized but still is perturbed by the alloy microstructure. The origin of the anomalous behavior of the hole GS energy of Config. 18, discussed in Sec. III B, can readily be inferred from Fig. 6. We find that, for this configuration, the hole GS is localized exceptionally high in the QW and directly below the WWF. Therefore, the hole state will be significantly affected by local changes in the built-in potential and strain field, introduced by the presence of a WWF (cf. discussion in Sec. III A). This extreme situation results in the feature observed in Fig. 2, that Config. 18 exhibits a slight decrease in hole GS energy with the inclusion of the WWF, in contrast to all other configurations. Furthermore, the spatial separation, both in and out of the growth plane, of electron and hole wave functions is unusually small. This leads to an exceptionally large exciton binding energy (cf. Fig. 5).

To further elucidate the connection between carrier-localization features and wave-function overlap, we have calculated the single-particle emission spectrum for Configs. 4 and 11 in the presence and absence of the WWF. The results are displayed in Fig. 7. We do not present here the results from Config. 18, since the oscillator strength in this case is more than 20 times larger than the largest value of Config. 11. This feature would distract here from the results of the more "standard" configurations. In the following, all data are normalized to the results from Config. 11 in the presence of the WWF. For visualization purposes, each peak has been broadened by a Gaussian function. As we can see from Fig. 7, the oscillator strength is approximately unchanged in the case of Config. 4 when adding or removing the WWF. For Config. 11, the hole wave function is localized near the WWF, explaining why in this case the oscillator strength is higher when the WWF is present compared to the case without the WWF (cf. Fig. 7).

In a second step, we study now how the (attractive) Coulomb interaction affects the results. These data are shown on the right-hand side of Fig. 6 (Many-Body) with and without the WWF. When comparing these results with the single-particle data, in the presence of the WWF, very little change is observed in the spatial localization features of both electrons and holes. This means that electron and holes are basically "independently" localized. For the case where there is no WWF, we may still say that the electron and hole are independently localized on opposite interfaces of the QW; however, more pronounced charge-density rearrangements for the electron are observed. This lateral rearrangement of the electron charge density can most easily be seen from the top view. In both cases (Configs. 4 and 11), these redistributions of the electron charge density about the hole wave function should lead to a (slight) increase in the GS oscillator strength. The calculated excitonic GS emission spectrum is shown in Fig. 8. Indeed for Configs. 11 and 4, the attractive Coulomb interaction leads in both cases, with and without WWFs, to a slight increase slight increase in oscillator strength and to a redshift in the

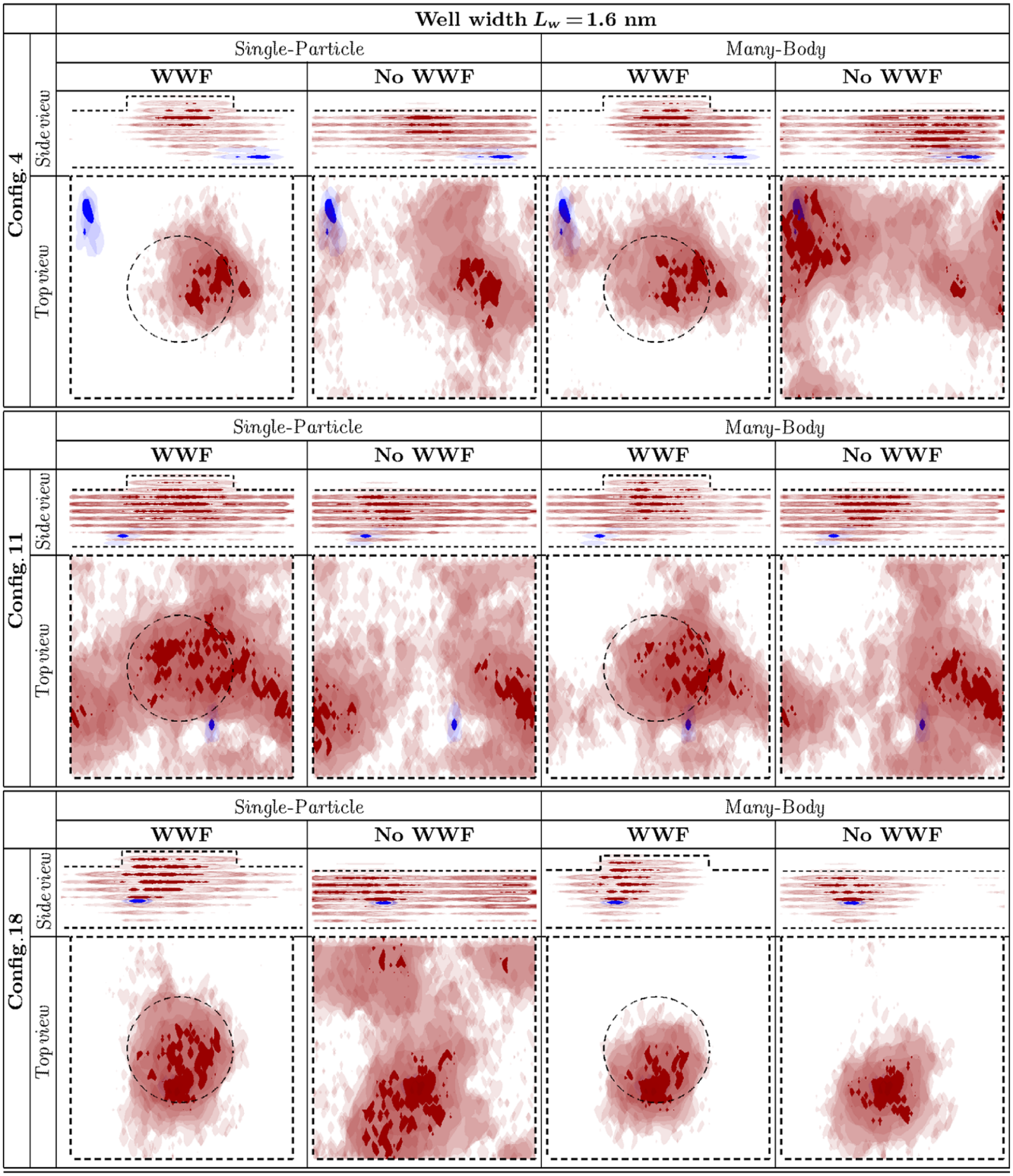


FIG. 9. Isosurface plots of electron (red) and hole (blue) ground-state charge densities in the absence (Single-Particle, left) and presence (Many-Body, right) of Coulomb (excitonic) effects for different microscopic configurations and different viewpoints. The side view is perpendicular to the c-axis, and the top view is parallel to the c-axis. The light (dark) isosurfaces correspond to 10% (50%) of the maximum charge density. Results are shown with (WWF) and without (No WWF) well-width fluctuations. The well width L_w here is $L_w = 1.6$ nm.

emission energies. Note here that the data are again normalized to Config. 11 in the absence of Coulomb effects but in the presence of the WWF (cf. Fig. 7). The finding that, with and without WWFs, we observe only slight changes in the oscillator strength is also consistent with the observation that, for larger well widths, the exciton binding energy does not change significantly (cf. Fig. 5) between the two systems (No WWF vs WWF).

Taking these results together with the observations on the exciton-binding energies (Fig. 5), one can draw the following conclusion: For larger QWs, the exciton binding energy is basically independent of lateral localization features. This can readily be inferred from Configs. 4 and 11 in Fig. 6, where we observe that, despite the noticeable difference in in-plane separation between the cases with and without WWFs, the differences in the binding energies are negligible. Furthermore, we find here that Config. 18 has the largest binding energy (cf. Fig. 5) of all configurations due to the smallest spatial separation of electron and hole GS wave functions. Also from the comparison of Figs. 7 and 8, we can deduce that the Coulomb effect is of secondary importance for the wave-function overlap, at least for larger well widths. However, the data indicate that, in general, reducing the QW barrier interface roughness and therefore WWFs should, even for these larger QW widths, allow for a redistribution of the (electron) charge density due to Coulomb effects. This finding already gives an indication that Coulomb effects can reduce the spatial in-plane separation of the carriers. Overall, the oscillator strength should at least slightly benefit from this feature.

Having discussed the $L_w = 3.43$ nm case, we now turn to the QW system with $L_w = 1.6$ nm. From Figs. 4 and 5, we know already that, compared to the system with $L_w = 3.43$ nm, the exciton binding energy is increased in the $L_w = 1.6$ nm structures on average. Also, in Fig. 5, we observe that both WWFs and the microscopic alloy structure lead to a significant variation in the exciton binding energy. To understand these differences, we look first at the electron and hole GS charge densities. These densities are presented in Fig. 9, using the same configurations as in Fig. 6.

We begin our analysis, as before, by looking at the single-particle properties (first two columns). Note that, for each configuration, the hole charge densities are essentially the same as in the $L_w = 3.43$ nm case, originating from the fact that, for a given configuration, the alloy microstructure at the lower interface of the well is unchanged when increasing the well width (cf. Sec. II B). The GS electron charge densities, being subject to a different atomic environment, show noticeable differences from the QW with $L_w = 3.43$ nm. However, the general behavior is similar, with the electron being strongly affected by the combined effect of built-in field and WWFs. Because of the smaller QW width, electron and hole wave functions are less vertically separated, leading to a higher spatial overlap between

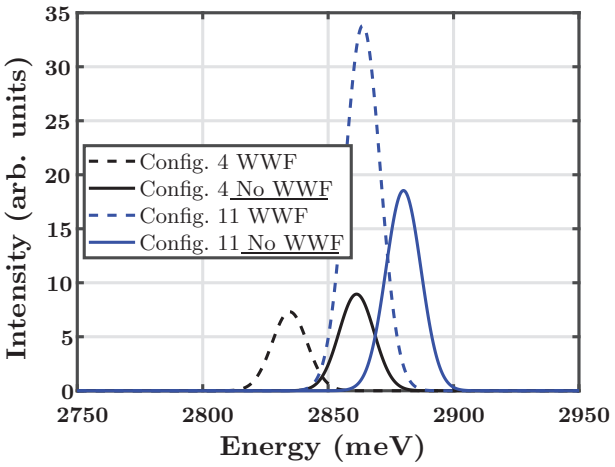


FIG. 10. Emission spectrum, neglecting Coulomb effects (single-particle), for Configs. 4 (black) and 11 (blue) in the presence (dashed lines) and absence (solid lines) of well-width fluctuations. The well width of the system is $L_w = 1.6$ nm. The data are normalized to the spectrum of Config. 11 in the absence of Coulomb effects but in the presence of the well-width fluctuation (WWF) (cf. Fig. 7).

the wave functions. This higher wave function overlap is also reflected in the calculated single-particle GS emission spectrum shown in Fig. 10, again for Configs. 4 and 11 with and without WWFs. As before, these data are normalized to the spectrum of Config. 11 for the well with $L_w = 3.43$ nm in the absence of Coulomb effects but in the presence of the WWF (cf. Fig. 7). Comparing the results for a well width of $L_w = 1.6$ nm (Fig. 10) with data for $L_w = 3.43$ nm (Fig. 7), we see that the oscillator strength increases by a factor of order of at least 20. Otherwise, the general features between the two systems are very similar. However, because of the increased spatial electron and hole wave function overlap and consistent with previous discussion, the exciton binding energy is significantly increased for the well with $L_w = 1.6$ nm when compared to the $L_w = 3.43$ nm system (cf. Fig. 5).

For the well with $L_w = 1.6$ nm, a pertinent question now relates to the balance between the enhanced Coulomb effect and the localization "strength" of WWF and random alloy: Is the Coulomb interaction strong enough at this width to overcome the localizing potential of the WWF and mitigate the lateral separation between the electron and hole? To investigate this, we consider the charge densities obtained in the presence of Coulomb effects. These results are shown in the last two columns of Fig. 9 (Many-Body). Initially, we focus our attention on the situation with WWFs. Looking at Config. 4, and comparing with the data from $L_w = 3.43$ nm (Fig. 6), we observe clearly a stronger redistribution of the electron charge density toward the hole. Similar findings hold for Configs. 11 and 18. However, the carrier-localization effects are still largely determined by random-alloy contributions and WWFs. In the

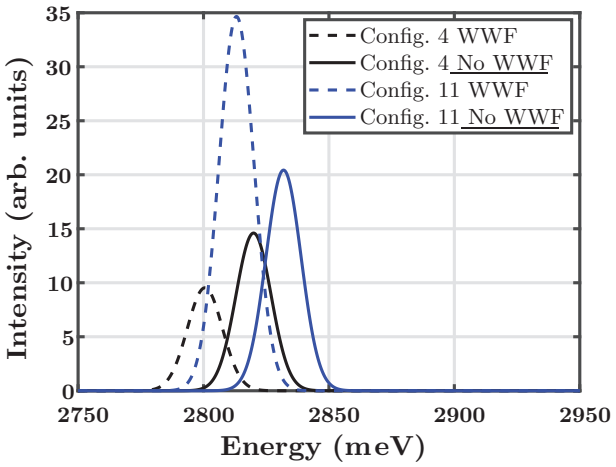


FIG. 11. Excitonic emission spectrum for Configs. 4 (black) and 11 (blue) in the presence (dashed lines) and absence (solid lines) of well-width fluctuations. The well width of the system is $L_w = 1.6$ nm. The data are normalized to the spectrum of Config. 11 in the absence of Coulomb effects but in the presence of the well-width fluctuation (WWF).

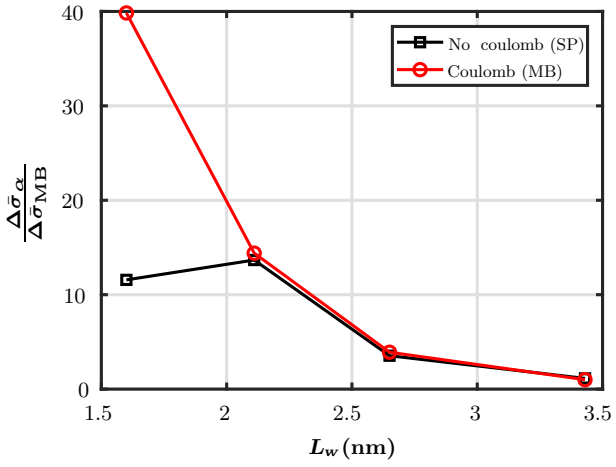


FIG. 12. Normalized difference in the average peak oscillator strength, $\Delta\bar{\sigma}_\alpha(L_w)$, between the system without and with the WWFs as a function of the well width L_w. The results are shown in the presence (red circle) and absence (black squares) of Coulomb effects. More details are given in the text.

presence of WWFs, even for the lowest well width studied here and independent of the microscopic configuration, the single-particle picture still gives a very good approximation of the system in terms of its localization features. Thus, this system is still consistent with the picture of "independently" localized carriers, as introduced by Morel *et al.* [2]. But, when looking at the corresponding excitonic emission spectrum (Fig. 11) and comparing to the single-particle emission spectrum (Fig. 10), we see that, even in the presence of WWFs (dashed lines), the oscillator strength is noticeably affected by the attractive Coulomb effect. Note again that the data are normalized to the spectrum of Config. 11 from Fig. 7. We will come back to the impact of the interplay of Coulomb effects and WWFs on the wave-function overlap in more detail below.

Taking the results from the $L_w = 3.53$ nm and $L_w = 1.6$ nm cases together, we are left with the following picture. Our calculations indicate that the importance of the Coulomb interaction depends strongly on the vertical separation of the electron and hole wave functions, and thus, in our case here, on the QW width. However, a similar effect would be observed with increasing In content, given that the strain-dependent piezoelectric potential increases with increasing In content and thus leads to a stronger out-of-plane separation of the carrier wave functions [59]. This statement is supported by our recent studies, where we have shown that, with increasing In content, carrier-localization effects of electrons and holes at the QW barrier interface are further enhanced and the out-of-plane carrier separation is increased [10]. Furthermore, we find here that WWFs serve as a barrier to the lateral charge-density redistribution facilitated by Coulomb effects.

However, the situation is less clear cut when WWFs are absent. For the largest well width considered here, $L_w = 3.43$ nm, charge-density redistributions are observed but, for instance, the oscillator strength or the exciton binding energies are only slightly affected. But, when the well width is reduced, these charge redistributions due to Coulomb effects are more pronounced and can partially compensate the in-plane carrier separation.

This argument is supported by the data displayed in Fig. 12, which shows the (normalized) difference in the average peak oscillator strength, $\Delta\bar{\sigma}_\alpha(L_w)/\Delta\bar{\sigma}_{\rm MB}(L_w = 3.43\ \text{nm}) = [\bar{\sigma}_\alpha^{\text{No WWF}}(L_w) - \bar{\sigma}_\alpha^{\text{WWF}}(L_w)]/[\bar{\sigma}_{\rm MB}^{\text{No WWF}}(L_w = 3.43\ \text{nm}) - \bar{\sigma}_{\rm MB}^{\text{WWF}}(L_w = 3.43\ \text{nm})]$, between the system without (No WWF) and with WWFs. The results are shown as a function of the well width L_w. The index α denotes if the calculations have been performed in the presence (MB, red circles) or absence (SP, black squares) of Coulomb effects. Here, the data are normalized to $\Delta\bar{\sigma}_{\rm MB}(L_w = 3.43\ \text{nm})$. Figure 12 reveals that, for the largest well width, removing the WWF has very little effect on the oscillator strength $[\Delta\bar{\sigma}_\alpha(L_w = 3.43\ \text{nm})/\Delta\bar{\sigma}_{\rm MB}(L_w = 3.43\ \text{nm}) \approx 1]$. However, with decreasing well width L_w, $\Delta\bar{\sigma}_\alpha/\Delta\bar{\sigma}_{\rm MB} \gg 1$, indicating that the oscillator strength in the absence of the WWF increases on average much more quickly when compared to the situation where the WWF is present. This finding holds also for the situation with and without Coulomb effects. Note that the kink in the data without Coulomb effects (black squares) is caused by the extreme configuration 18. When neglecting config. 18 (not shown), $\Delta\bar{\sigma}_{\rm SP}(L_w = 1.6\ \text{nm})/\Delta\bar{\sigma}_{\rm MB}(L_w = 3.43\ \text{nm}) \approx 16$ and $\Delta\bar{\sigma}_{\rm SP}(L_w = 2.11\ \text{nm})/\Delta\bar{\sigma}_{\rm MB}(L_w = 3.43\ \text{nm})$ decrease slightly. Overall, our analysis strengthens the argument that reducing the roughness of the QW barrier interface

can have a significant impact on the optical properties of (In,Ga)N/GaN QWs and thus on devices utilizing these systems. We discuss these benefits in more detail in the following section.

D. Comparison with experiment and consequences for radiative recombination in (In,Ga)N/GaN quantum wells

Taking all the above into account, we can draw the following conclusions, which are relevant for the radiative recombination dynamics and optical properties of (In,Ga)N/GaN QWs. Looking at Fig. 12 we note here that in the extreme case of low well width and no WWFs, Coulomb effects have a very strong impact on $\Delta\bar{\sigma}_{\mathrm{MB}}(L_w)/\Delta\bar{\sigma}_{\mathrm{MB}}(L_w = 3.43\ \mathrm{nm})$, reflecting the above discussed observation that, in the absence of WWFs, the spatial in-plane separation can be reduced by the Coulomb effect. This finding has two immediate consequences.

First, if the green-gap problem is related to in-plane carrier-localization effects, as argued in Refs. [11,13], reducing the surface roughness of GaN on (In,Ga)N might lead to a significant improvement in the device performance, at least for the radiative recombination, given the charge-density redistribution due to Coulomb effects and the connected reduction of the spatial in-plane separation. Our finding here is in line with the recent experimental studies focusing on this topic [55,60,61]. Our calculations confirm and support the recent experimental arguments that understanding and tailoring the QW barrier interface in terms of roughness plays an important role in the tuning of the electronic and optical properties of these systems. Furthermore, our argument that the interface roughness plays a key role for optical properties of these systems might also be related to the experimentally reported enhancement of the PL intensity of (In,Ga)N/GaN QWs after reduction of the surface roughness via hydrogen treatment during growth [62].

In addition to these device-related aspects, our above presented results indicate also potential changes in the fundamental physical properties of the radiative recombination dynamics of (In,Ga)N/GaN QWs with varying well width. Here, we find for instance that for some configurations the recombination process may be considered as being driven by exciton localization effects (cf. configs. 4 and 18 in Fig. 9), with the electron localizing about the hole, instead of a picture of independently localized carriers. Reducing the well width and/or the In content further, and thus the built-in field, might lead to the situation of exciton localization in general, independent of the microscopic configuration. Therefore, our results give indications that a continuous transition from a system that can be described by independently localized carriers to the case where radiative recombination is determined by exciton localization effects may be achieved. Experimentally such a transition could be observed by changes in the time-dependent PL decay curves. For instance, a non-single-exponential decay in *c*-plane (In,Ga)N/GaN QWs has often been explained by the picture of independently localized carriers [2,9]. For nonpolar systems, single-exponential decay curves have been measured and exciton localization effects have been used to explain this behavior [9,63,64]. Interestingly, such an effect of a change in PL decay characteristics has been observed experimentally by Davidson *et al.* [31] and Langer *et al.* [65] in *c*-plane systems. In the experiments of Davidson *et al.* [31], the well width of *c*-plane (In,Ga)N/GaN QWs with 13% In has been reduced from 5 to 1.25 nm, revealing the transition from nonexponential to single-exponential decay curves. In the study of Langer *et al.* [65], a marked difference in the carrier dynamics of 2.7- and 1.1-nm QWs is observed, with the constancy of the PL decay lifetime of the smaller well with carrier density imputed to strong excitonic effects.

Furthermore, Langer *et al.* [65], as well as Hangleiter *et al.* [66], discussed in their work excitonic recombination at room temperature. To achieve such a behavior, large exciton binding energies, exceeding the room-temperature thermal energy of 26 meV, are required. Exciton binding energies of 15–50 meV have been reported in combined theoretical and experimental literature studies on GaN and (In,Ga)N QWs [67,68]. These values are in good agreement with our obtained values of 30–50 meV (cf. Fig. 5) for $In_{0.15}Ga_{0.85}N$/GaN QWs. Therefore, the exciton binding energies calculated here, which exceed the thermal energy at room temperature, might facilitate the existence of stable excitons at room temperature as reported experimentally.

IV. CONCLUSION

In summary, we have presented a detailed theoretical analysis of the impact of the interplay among well width, structural inhomogeneities, alloy fluctuations, and Coulomb effects on the electronic and optical properties of (In,Ga)N/GaN QWs. This analysis not only gave insight into fundamental properties of this material system, but also revealed possible routes toward the optimization of the radiative recombination process in (In,Ga)N-based devices via tailoring their structural properties.

Overall, our calculations reveal that for the QW widths L_w studied here, ranging from $L_w = 1.6$ nm up to $L_w = 3.43$ nm, carrier-localization effects due to built-in field, well-width fluctuations (electrons), and random-alloy fluctuations (holes) dominate over the attractive Coulomb interaction between the carriers. At least in terms of wave-function-localization features, we are left with the picture of "independently" localized carriers, consistent

with the model introduced by Morel *et al.* [2] to explain time-resolved PL-spectra of *c*-plane (In,Ga)N/GaN QWs.

Our data also show that if well-width fluctuations are present, in addition to the built-in-field-induced, out-of-plane wave-function separation, an additional in-plane component is present. This component is only slightly affected when Coulomb effects are taken into account. Auf der Maur *et al.* [11] argued that this in-plane separation feature is a significant component of the "green gap," though their calculations neglected well-width fluctuations and Coulomb effects.

However, our study shows that, in the absence of structural inhomogeneities such as well-width fluctuations, the situation is less clear cut. In this case, and neglecting Coulomb effects initially, carrier-localization effects are introduced by the interplay of random-alloy fluctuations and built-in field. Here, we find that hole wave functions are strongly localized by the random-alloy fluctuations, while the electron wave functions are more delocalized when compared to the situation with a well-width fluctuation. But, the electron wave function, in terms of localization features, is only perturbed by the random-alloy fluctuations. Thus, this gives rise to an in-plane spatial separation of electron and hole wave functions. When including Coulomb effects in the calculations, for larger well width, only slight modifications of the charge densities are observed. However, these results indicated a charge-density redistribution of the electron wave function, while the hole charge density is basically unchanged. This feature is more pronounced with decreasing well width, clearly revealing that, in the absence of well-width fluctuations, the in-plane spatial separation of electron and hole wave functions in a single-particle picture can be reduced by the attractive Coulomb interaction between the carriers.

Therefore, our analysis gives the important finding that reducing the GaN (In,Ga)N interface roughness in (In,Ga)N/GaN QWs should be extremely beneficial for the radiative recombination in light emitters utilizing this material system. This originates from the observation that, in the absence of well-width fluctuations, the in-plane spatial carrier localization can be partially compensated by the attractive Coulomb interaction.

While these features are of interest from a device-application point of view, especially for the green-gap problem, our results also indicate that it might be possible to "tune the physics" of this system by changing the well width. For instance, we observe here that, for the smallest well width ($L_w = 1.6$ nm), for some configurations, the electron localizes about the hole due to the attractive Coulomb interaction. Thus, we observe here exciton localization features in *c*-plane structures instead of the picture of "independently" localized carriers usually used to describe the optical properties of these systems. Experimentally, such a transition could be observed in time-resolved PL measurements, for instance, and has indeed been measured in *c*-plane systems [31,65]. Moreover, our analysis presented here, in terms of carrier localization and the impact of Coulomb effects, should also be of interest for studies on monolayer (In,Ga)N/GaN systems [69].

ACKNOWLEDGMENTS

This work was supported by Science Foundation Ireland (Grant No. 13/SIRG/2210).

[1] Y.-H. Cho, G. H. Gainer, A. J. Fischer, J. J. Song, S. Keller, U. K. Mishra, and S. P. DenBaars, "S-shaped" temperature-dependent emission shift and carrier dynamics in InGaN/GaN multiple quantum wells, Appl. Phys. Lett. **73**, 1370 (1998).

[2] A. Morel, P. Lefebvre, S. Kalliakos, T. Taliercio, T. Bretagnon, and B. Gil, Donor-acceptor-like behavior of electron-hole pair recombinations in low-dimensional (Ga,In)N/GaN systems, Phys. Rev. B **68**, 045331 (2003).

[3] D. M. Graham, A. Soltani-Vala, P. Dawson, M. J. Godfrey, T. M. Smeeton, J. S. Barnard, M. J. Kappers, C. J. Humphreys, and E. J. Thrush, Optical and microstructural studies of InGaN/GaN single-quantum-well structures, J. Appl. Phys. **97**, 103508 (2002).

[4] Shigefusa F. Chichibu, Akira Uedono, Takeyoshi Onuma, Benjamin A. Haskell, Arpan Chakraborty, Takahiro Koyama, Paul T. Fini, Stacoa Keller, Steven P. Denbaars, James S. Speck, Umesh K. Mishra, Shuji Nakamura, Shigeo Yamaguchi, Satoshi Kamiyama, Hiroshi Aamano, Isamu Akasaki, Jung Han, and Takayuki Sota, Origin of defect-insensitive emission probability in In-containing (Al,In,Ga)N alloy semiconductors, Nat. Mater. **5**, 810 (2006).

[5] D. Watson-Parris, M. J. Godfrey, P. Dawson, R. A. Oliver, M. J. Galtrey, M. J. Kappers, and C. J. Humphreys, Carrier localization mechanisms in $In_xGa_{1-x}N$/GaN, Phys. Rev. B **83**, 115321 (2011).

[6] S. Hammersley, D. Watson-Parris, P. Dawson, M. J. Godfrey, T. J. Badcock, M. J. Kappers, C. McAleese, R. A. Oliver, and C. J. Humphreys, The consequences of high injected carrier densities on carrier localization and efficiency droop in InGaN/GaN quantum well structures, J. Appl. Phys. **111**, 083512 (2012).

[7] T.-J. Yang, Ravi Shivaraman, James S. Speck, and Yuh-Renn Wu, The influence of random indium alloy fluctuations in indium gallium nitride quantum wells on the device behavior, J. Appl. Phys. **116**, 113104 (2014).

[8] Stefan Schulz, Miguel A. Caro, Conor Coughlan, and Eoin P. O'Reilly, Atomistic analysis of the impact of alloy and well-width fluctuations on the electronic and optical properties of InGaN/GaN quantum wells, Phys. Rev. B **91**, 035439 (2015).

[9] P. Dawson, S. Schulz, R. A. Oliver, M. J. Kappers, and C. J. Humphreys, The nature of carrier localisation in polar and nonpolar InGaN/GaN quantum wells, J. Appl. Phys. **119**, 181505 (2016).

[10] D. P. Tanner, M. A. Caro, E. P. O'Reilly, and S. Schulz, Random alloy fluctuations and structural inhomogeneities

in *c*-plane $In_xGa_{1-x}N$ quantum wells: Theory of ground and excited electron and hole states, RSC Adv. **6**, 64513 (2016).

[11] Matthias Auf der Maur, Alessandro Pecchia, Gabriele Penazzi, Walter Rodrigues, and Aldo Di Carlo, Efficiency Drop in Green InGaN/GaN Light Emitting Diodes: The Role of Random Alloy Fluctuations, Phys. Rev. Lett. **116**, 027401 (2016).

[12] C. M. Jones, C.-H. Teng, Q. Yan, P.-C. Ku, and E. Kioupakis, Impact of carrier localization on recombination in InGaN quantum wells and the efficiency of nitride light-emitting diodes: Insights from theory and numerical simulations, Appl. Phys. Lett. **111**, 113501 (2017).

[13] Sergey Yu. Karpov, Carrier localization in InGaN by composition fluctuations: Implication to the "green gap", Photon. Res. **5**, A7 (2017).

[14] M. Filoche, M. Piccardo, Y.-R. Wu, C.-K. Li, C. Weisbuch, and S. Mayboroda, Localization landscape theory of disorder in semiconductors. I. Theory and modeling, Phys. Rev. B **95**, 144204 (2017).

[15] C.-K. Li, M. Piccardo, L.-S. Lu, S. Mayboroda, L. Martinelli, J. Peretti, J. S. Speck, C. Weisbuch, M. Filoche, and Y.-R. Wu, Localization landscape theory of disorder in semiconductors. III. Application to carrier transport and recombination in light emitting diodes, Phys. Rev. B **95**, 144206 (2017).

[16] M. Piccardo, C.-K. Li, Y.-R. Wu, J. S. Speck, B. Bonef, R. M. Farrell, M. Filoche, L. Martinelli, J. Peretti, and C. Weisbuch, Localization landscape theory of disorder in semiconductors. II. Urbach tails of disordered quantum well layers, Phys. Rev. B **95**, 144205 (2017).

[17] M. A. Sousa, T. C. Esteves, N. B. Sedrine, J. Rodrigues, M. B. Lourenco, A. Redondo-Cubero, E. Alves, K. P. O'Donnell, M. Bockowski, C. Wetzel, M. R. Correia, K. Lorenz, and T. Monteiro, Luminescence studies on green emitting InGaN/GaN MQWs implanted with nitrogen, Sci. Rep. **5**, 9703 (2015).

[18] W. E. Blenkhorn, S. Schulz, D. S. P. Tanner, R. A. Oliver, M. J. Kappers, C. J. Humphreys, and P. Dawson, Resonant photoluminescence studies of carrier localisation in *c*-plane InGaN/GaN quantum well structures, J. Phys.: Condens. Matter **30**, 175303 (2018).

[19] Shigefusa Chichibu, Kazumi Wada, and Shuji Nakamura, Spatially resolved cathodoluminescence spectra of InGaN quantum wells, Appl. Phys. Lett. **71**, 2346 (1997).

[20] I. Ho and G. B. Stringfellow, Solid phase immiscibility in GaInN, Appl. Phys. Lett. **69**, 2701 (1996).

[21] T. M. Smeeton, M. J. Kappers, J. S. Barnard, M. E. Vickers, and C. J. Humphreys, Electron-beam-induced strain within InGaN quantum wells: False indium cluster detection in the transmission electron microscope, Appl. Phys. Lett. **83**, 5419 (2003).

[22] M. J. Galtrey, R. A. Oliver, M. J. Kappers, C. J. Humpreys, D. J. Stokes, P. H. Clifton, and A. Cerezo, Three-dimensional atom probe studies of an $In_xGa_{1-x}N$/GaN multiple quantum well structure: Assessment of possible indium clustering, Appl. Phys. Lett. **90**, 061903 (2007).

[23] S. Yu. Karpov, Suppression of phase separation in InGaN due to elastic strain, MRS Internet J. Nitride Semicond. Res. **3**, e16 (1998).

[24] George Sarau, Martin Heilmann, Michael Latzel, and Silke Christiansen, Disentangling the effects of nanoscale structural variations on the light emission wavelength of single nano-emitters: InGaN/GaN multiquantum well nano-leds for a case study, Nanoscale **6**, 11953 (2014).

[25] C.-K. Tan, W. Sun, J. J. Wierer, and N. Tansu, Effect of interface roughness on auger recombination in semiconductor quantum wells, AIP Adv. **7**, 035212 (2017).

[26] Emmanouil Kioupakis, Patrick Rinke, Kris T. Delaney, and Chris G. Van de Walle, Indirect auger recombination as a cause of efficiency droop in nitride light-emitting diodes, Appl. Phys. Lett. **98**, 161107 (2011).

[27] M. Binder, A. Nirschl, R. Zeisel, T. Hager, H.-J. Lugauer, M. Sabathil, D. Bougeard, J. Wagner, and B. Galler, Identification of nnp and npp auger recombination as significant contributor to the efficiency droop in (GaIn)N quantum wells by visualization of hot carriers in photoluminescence, Appl. Phys. Lett. **103**, 071108 (2013).

[28] Justin Iveland, Lucio Martinelli, Jacques Peretti, James S. Speck, and Claude Weisbuch, Direct Measurement of Auger Electrons Emitted from a Semiconductor Light-emitting Diode under Electrical Injection: Identification of the Dominant Mechanism for Efficiency Droop, Phys. Rev. Lett. **110**, 177406 (2013).

[29] B. Galler, H.-J. Lugauer, M. Binder, R. Hollweck, Y. Folwill, A. Nirschl, A. O. Gomez-Iglesias, B. Hahn, J. Wagner, and M. Sabathil, Experimental determination of the dominant type of auger recombination in InGaN quantum wells, Appl. Phys. Express **6**, 112101 (2013).

[30] D. T. S. Watson-Parris, PhD thesis, University of Manchester, 2011, https://www.escholar.manchester.ac.uk/ukacman-scw:132844.

[31] J. A. Davidson, P. Dawson, Tao Wang, T. Sugahara, J. W. Orton, and S. Sakai, Photoluminescence studies of InGaN/GaN multi-quantum wells, Semicond. Sci. Technol. **15**, 497 (2000).

[32] B. Monemar, J. P. Bergman, J. Dalfors, G. Pozina, B. E. Sernelius, P. O. Holtz, H. Amano, and I. Akasaki, Radiative recombination in $In_{0.15}Ga_{0.85}N$/GaN multiple quantum well structures, MRS Internet J. Nitride Semicond. Res. **4**, e16 (1999).

[33] Y. Narukawa, Y. Kawakami, S. Fujita, S. Fujita, and S. Nakamura, Recombination dynamics of localized excitons in $In_{0.20}Ga_{0.80}N$-$In_{0.05}Ga_{0.95}N$ multiple quantum wells, Phys. Rev. B **55**, R1938 (1997).

[34] Steven J. Plimpton, Fast parallel algorithms for short-range molecular dynamics, J. Comput. Phys. **117**, 1 (1995).

[35] Richard M. Martin, Elastic properties of ZnS structure semiconductors, Phys. Rev. B **1**, 4005 (1970).

[36] Miguel A. Caro, Stefan Schulz, and Eoin P. O'Reilly, Theory of local electric polarization and its relation to internal strain: Impact on polarization potential and electronic properties of group-III nitrides, Phys. Rev. B **88**, 214103 (2013).

[37] T. Saito and Y. Arakawa, Electronic structure of piezoelectric $In_{0.2}Ga_{0.8}N$ quantum dots in GaN calculated using a tight-binding method, Physica E **15**, 169 (2002).

[38] M. Zielinski, W. Jaskolski, J. Aizpurua, and G. W. Bryant, Strain and spin-orbit effects in self-assembled quantum dots, Acta Phys. Pol. A **108**, 929 (2005).

[39] K. Schuh, S. Barthel, O. Marquardt, T. Hickel, J. Neugebauer, G. Czycholl, and F. Jahnke, Strong dipole coupling in nonpolar nitride quantum dots due to Coulomb effects, Appl. Phys. Lett. **100**, 092103 (2012).

[40] N. Baer, S. Schulz, P. Gartner, S. Schumacher, G. Czycholl, and F. Jahnke, Influence of symmetry and Coulomb-correlation effects on the optical properties of nitride quantum dots, Phys. Rev. B **76**, 075310 (2007).

[41] Z. H. Levine and S. G. Louie, New model dielectric function and exchange-correlation potential for semiconductors and insulators, Phys. Rev. B **25**, 6310 (1982).

[42] A. Franceschetti, H. Fu, L. W. Wang, and A. Zunger, Many-body pseudopotential theory of excitons in InP and CdSe quantum dots, Phys. Rev. B **60**, 1819 (1999).

[43] S. Nakamura and S. F. Chichibu, eds., *Introduction to Nitride Semiconductor Blue Lasers and Light Emitting Diodes* (CRC Press, London and New York, 2000).

[44] V. Yu Davydov, A. A. Klochikhin, M. B. Smirnov, V. V. Emtsev, V. D. Petrikov, I. A. Abroyan, A. I. Titov, I. N. Goncharuk, A. N. Smirnov, V. V. Mamutin, S. V. Ivanov, and T. Inushima, Phonons in hexagonal InN. Experiment and theory, Phys. Status Solidi B **216**, 779 (1999).

[45] M. Swiderski and M. Zielinski, Atomistic theory of excitonic fine structure in InAs/InP nanowire quantum dot molecules, Phys. Rev. B **95**, 125407 (2017).

[46] W. Sheng, S.-J. Cheng, and P. Hawrylak, Multiband theory of multi-exciton complexes in self-assembled quantum dots, Phys. Rev. B **71**, 035316 (2005).

[47] E. Goldmann, S. Barthel, M. Florian, K. Schuh, and F. Jahnke, Excitonic fine-structure splitting in telecom-wavelength InAs/GaAs quantum dots: Statistical distribution and height-dependence, Appl. Phys. Lett. **103**, 242102 (2013).

[48] S. Schulz, S. Schumacher, and G. Czycholl, Tight-binding model for semiconductor quantum dots with a wurtzite crystal structure: From one-particle properties to Coulomb correlations and optical spectra, Phys. Rev. B **73**, 245327 (2006).

[49] Mark J. Galtrey, Rachel A. Oliver, Menno J. Kappers, and Colin J. Humphreys, Three-dimensional atom probe studies of an $In_xGa_{1-x}N/GaN$ multiple quantum well structure: Assessment of possible indium clustering, Appl. Phys. Lett. **90**, 061903 (2007).

[50] P. M. McBride, Q. Yan, and C. G. VandeWalle, Effects of in profile on simulations of InGaN/GaN multi-quantum-well light-emitting diodes, Appl. Phys. Lett. **105**, 083507 (2014).

[51] B. Monemar, J. P. Bergman, J. Dalfors, G. Pozina, B. E. Sernelius, P. O. Holtz, H. Amano, and I. Akasaki, Radiative recombination in $In_{0.15}Ga_{0.85}N/GaN$ multiple quantum well structures, MRS Internet J. Nitride Semicond. Res. **4**, e16 (1999).

[52] L. Hoffmann, H. Bremers, H. Jönen, U. Rossow, M. Schowalter, T. Mehrtens, A. Rosenauer, and A. Hangleiter, Atomic scale investigations of ultra-thin GaInN/GaN quantum wells with high indium content, Appl. Phys. Lett. **102**, 102110 (2013).

[53] R. A. Oliver, S. E. Bennett, T. Zhu, D. J. Beesley, M. J. Kappers, D. W. Saxey, A. Cerezo, and C. J. Humphreys, Microstructural origins of localization in InGaN quantum wells, J. Phys. D: Appl. Phys. **43**, 354003 (2010).

[54] T. Sato, K. Nakano, H. Matsumoto, S. Torikawa, I. Nakatani, M. Kiyohara, and T. Isshiki, High quality lamella preparation of gallium nitride compound semiconductor using Triple BeamTM system, J. Phys.: Conf. Ser. **902**, 012019 (2017).

[55] F. Massabuau, N. Piot, M. Frentrup, X. Wang, Q. Avenas, M. Kappers, C. Humphreys, and R. Oliver, X-ray reflectivity method for the characterization of InGaN/GaN quantum well interface, Phys. Status Solidi B **254**, 1600664 (2017).

[56] S. F. Chichibu, A. C. Abare, M. S. Minsky, S. Keller, S. B. Fleischer, J. E. Bowers, E. Hu, U. K. Mishra, L. A. Coldren, S. P. DenBaars, and T. Sota, Effective band gap inhomogeneity and piezoelectric field in InGaN/GaN multiquantum well structures, Appl. Phys. Lett. **73**, 2006 (1998).

[57] K. P. O'Donnell, R. W. Martin, and P. G. Middleton, Origin of Luminescence from InGaN Diodes, Phys. Rev. Lett. **82**, 237 (1999).

[58] S. Barthel, K. Schuh, O. Marquardt, T. Hickel, J. Neugebauer, F. Jahnke, and G. Czycholl, Interplay between Coulomb interaction and quantum-confined stark-effect in polar and nonpolar wurtzite InN/GaN quantum dots, Eur. Phys. J. B **86**, 449 (2013).

[59] D. P. Williams, S. Schulz, A. D. Andreev, and E. P. O'Reilly, Theory of GaN quantum dots for optical applications, J. Sel. Top. Quant. Electron. **15**, 1092 (2009).

[60] Y.-C. Cheng, C.-M. Wu, M.-K. Chen, C. C. Yang, and Z.-C. Feng, Improvements of InGaN/GaN quantum-well interfaces and radiative efficiency with InN interfacial layers, Appl. Phys. Lett. **84**, 5422 (2004).

[61] Z. Wu, X. Shen, H. Xiong, Q. Li, J. Kang, Z. Fang, F. Lin, B. Yang, S. Lin, W. Shen, and T.-Y. Zhang, Improved interface quality and luminescence capability of InGaN/GaN quantum wells with Mg pretreatment, Appl. Phys. A **122**, 108 (2016).

[62] Yadan Zhu, Taiping Lu, Xiaorun Zhou, Guangzhou Zhao, Hailiang Dong, Zhigang Jia, Xuguang Liu, and Bingshe Xu, Effect of hydrogen treatment temperature on the properties of InGaN/GaN multiple quantum wells, Nanoscale Res. Lett. **12**, 321 (2017).

[63] S. Marcinkevicius, K. M. Kelchner, L. Y. Kuritzky, S. Nakamura, S. P. DenBaars, and J. S. Speck, Photoexcited carrier recombination in wide *m*-plane InGaN/GaN quantum wells, Appl. Phys. Lett. **103**, 111107 (2013).

[64] S. Schulz, D. P. Tanner, E. P. O'Reilly, M. A. Caro, T. L. Martin, P. A. J. Bagot, M. P. Moody, F. Tang, J. T. Griffiths, F. Oehler, M. J. Kappers, R. A. Oliver, C. J. Humphreys, D. Sutherland, M. J. Davies, and P. Dawson, Structural, electronic, and optical properties of *m*-plane InGaN/GaN quantum wells: Insights from experiment and atomistic theory, Phys. Rev. B **92**, 235419 (2015).

[65] T. Langer, A. Chernikov, D. Kalincev, M. Gerhard, H. Bremers, U. Rossow, M. Koch, and A. Hangleiter, Room temperature excitonic recombination in GaInN/GaN quantum wells, Appl. Phys. Lett. **103**, 202106 (2013).

[66] A. Hangleiter, Z. Jin, M. Gerhard, D. Kalincev, T. Langer, H. Bremers, U. Rossow, M. Koch, M. Bonn, and D. Turchinovic, Efficient formation of excitons in a dense electron-hole plasma at room temperature, Phys. Rev. B **92**, 241305(R) (2015).

[67] P. Bigenwald, P. Lefebvre, T. Bretagnon, and B. Gil, Confined excitons in GaN/AlGaN quantum wells, Phys. Status Solidi (b) **216**, 371 (1999).

[68] S. Lahmann, F. Hitzel, U. Rossow, and A. Hangleiter, Analysis of quantum efficiency of high brightness GaInN/GaN quantum wells, Phys. Status Solidi (c) **0**, 2202 (2003).

[69] D. Ma, X. Rong, X. Zheng, W. Wang, P. Wang, T. Schulz, M. Albrecht, S. Metzner, M. Müller, O. August, F. Bertram, J. Christen, P. Jin, M. Li, J. Zhang, X. Yang, F. Xu, Z. Qin, W. Ge, B. Shen, and X. Wang, Exciton emission of quasi-2d InGaN in GaN matrix grown by molecular beam epitaxy, Sci. Rep. **7**, 46420 (2017).